buildings

MDPI

Article

An Improved Anchorage System for L-Shaped FRP Composites to Enhance the Seismic Response of Beam-Column Joints in a Low-Strength Substandard Reinforced Concrete (RC) Frame

Waqas Adil [1,*], Fayyaz Ur Rahman [1], Qaisar Ali [1] and Christos G. Papakonstantinou [2,*]

[1] Department of Civil Engineering, University of Engineering and Technology, Peshawar 25120, Pakistan; engrfayyaz@uetpeshawar.edu.pk (F.U.R.); drqaisarali@uetpeshawar.edu.pk (Q.A.)
[2] Laboratory of Concrete Technology and Reinforced Concrete Structures, Department of Civil Engineering, University of Thessaly, 38334 Volos, Greece
* Correspondence: engrwaqasadil@uetpeshawar.edu.pk (W.A.); cpapak@uth.gr (C.G.P.); Tel.: +30-698-444-0253 (C.G.P.)

Abstract: Reinforced concrete buildings are prone to collapse during seismic events due to the brittle shear failure of non-seismic beam-column joints (BCJ). In this study, two one-third scale reinforced concrete (RC) frames incorporating various non-seismic details were tested under lateral cyclic loading. One of the RC frames was used as control, while the other was strengthened using externally bonded carbon-fiber-reinforced polymer (CFRP) sheets in a L-Shaped configuration with particular attention to anchorage to evade debonding. For the strengthening process, L-shaped CFRP sheets were bonded to the inner face of columns, extended on beams both above and below the joint up to a hinge length. To avert debonding, the L-shaped CFRP sheets were fully wrapped with CFRP sheets around the column, both near the joint and at the end of the sheet. The sheets were also wrapped around the beam, through two slots in the slab that were adjacent to the beam-column interface and at the far end of the sheet. Test results confirmed that the installation of CFRP sheets in an L-shaped configuration altered the brittle-shear failure mechanism of the beam-column joints to a ductile failure by repositioning the hinges away from the columns. Additionally, the proposed anchorage method successfully eradicated the debonding and peel-off of the CFRP sheets. Moreover, strengthening with the CFRP sheets in the L-shaped configuration enhanced the strength and ductility of the RC frame by 45% and 43%, respectively. According to the findings of this study, the application of L-shaped CFRP sheets proved effective in strengthening RC frame structures.

Keywords: CFRP sheets; BCJ; L-shaped CFRP; FRP composites; anchorage; debonding; seismic strengthening; reinforced concrete; RC frame

Citation: Adil, W.; Rahman, F.U.; Ali, Q.; Papakonstantinou, C.G. An Improved Anchorage System for L-Shaped FRP Composites to Enhance the Seismic Response of Beam-Column Joints in a Low-Strength Substandard Reinforced Concrete (RC) Frame. *Buildings* **2024**, *14*, 721. https://doi.org/10.3390/buildings14030721

Academic Editor: Jaroslav Pokorný

Received: 16 February 2024
Revised: 3 March 2024
Accepted: 5 March 2024
Published: 7 March 2024

1. Introduction

Most reinforced concrete (RC) structures built before 1980 do not satisfy the up-to-date seismic code requirements. Along with other deficiencies, non-seismic detailing of reinforcement in the beam-column joints (BCJ) is a primary reason for brittle shear failure. BCJ is the main component that plays a key role in controlling the overall strength, ductility, and stability of the structure; hence, the undesirable brittle failure mode of BCJ results in a catastrophic collapse of buildings during ground motions [1,2]. Despite the code-compliant design, some modern RC structures also exhibit non-ductile failure of columns [3,4]. In such circumstances, it is crucial to implement an effective rehabilitation scheme to alter a brittle failure mode into a ductile failure mechanism.

Several conventional schemes were employed to rehabilitate beam–column connections, including RC jacketing [5], shotcrete jacketing [6], stiffened steel plates [7], steel cages [8–10], steel angles connected by bars [11,12], steel diagonal bolts [13], epoxy injection [14], and use of the ultra-high-performance concrete (UHPC) [15]. The implemented strengthening techniques proved effective in improving the seismic characteristics of BCJ.

Fiber-reinforced polymer (FRP) composites are rigorously used as externally bonded reinforcement (EBR) to rehabilitate the RC members. The growing interest in using FRP composites for rehabilitation is attributed to their most favorable characteristics, such as higher strength/weight ratio, light weight, resistance against corrosion, and availability in many forms to suit any cross-section [16–18]. Furthermore, FPR composites exhibit superior performance in addressing diverse challenges associated with RC members. This includes improving the fatigue life of concrete beams and preventing the deterioration of bond strength in highly corroded RC members, to name a few examples [19,20].

Numerous experimental studies on the FRP-rehabilitated RC structures have shown the efficacy of FRP systems in enhancing the strength and ductility-related features of different seismically deficient RC structures [16,21–26]. For instance, Antonopoulos and Triantafillou [16] conducted an extensive experimental investigation to assess the impact of different parameters, including no FRP ply, distribution of FRP on beam and column, carbon FRP (CFRP) vs. glass FRP (GFRP) fibers composites, initial damage, presence of transverse reinforcement in joint, axial load increment, and mechanical anchorage on the efficiency of FRP composites used in beam-column connections. It was concluded that the FRP composites, when properly bonded to a concrete surface, can enhance the strength, energy dissipation, and stiffness of BCJ that lacked shear reinforcement in the joint region. Furthermore, it was suggested that increasing the amount of FRP ply in the beam, applying a higher axial load on the column, and providing proper mechanical anchorage to FRP composites positively impacted seismic capacity enhancement. Anchoring is highly important to utilize the maximum capacity of FRP composites without debonding from the concrete substrate. This is evident from earlier studies on shear strengthened concrete beams [27,28]. Ghobarah et al. evaluated the performance of FRP composites in shear-deficient joints [26] and shear/anchorage-deficient joints [21]. It was concluded that the FRP composites abolished the brittle shear failure and slip of the inadequate bars as well as debonding when the FRP sheets were anchored by steel plates. To eliminate debonding, Elaheh Ilia and Davood Mostofinejad [22] strengthened the strong beam–weak column joints with different X-shaped FRP sheet configurations bonded to concrete surfaces using the externally bonded reinforcement on grooves (EBROG) method coupled with wrapping and FRP fans. The proposed retrofitting schemes substantially enhanced lateral load-carrying capacity, ductility, and energy dissipation capacity of the strengthened joints. N. Attari et.al [23] tested three beam–column joints strengthened with CFRP laminate on beam and L-shaped GFRP sheet for anchoring purposes. The test results suggested that the L-shaped anchoring scheme proved to be successful in delaying the failure of CFRP laminates and enhanced the lateral strength along with ductility. Le-Trung et al. [24] investigated the seismically deficient BCJ strengthened with the FRP composites applied in various configurations. The main idea was to assess the efficiency of the FRP systems to enhance the load-carrying potential and to avoid debonding by applying CFRP sheets in T, L, and X-shaped configurations. The research concluded that all configurations employed effectively improved the load-carrying capacity and ductility of the BCJ. Among all the configurations, the X-shaped layout proved to be the most efficient for enhancing the strength and ductility characteristics of seismically deficient BCJ. Halil Sezan [25] repaired the damaged beam-column joints with non-shrink mortar and applied FRP sheets in U-shaped along with X-shaped layouts and self-tapping screws for anchorage. Overall, the retrofitting scheme restored the strength and enhanced deformation capacity.

Similarly, the unavoidable construction joints, generally provided below and above the BCJ core, considerably reduce the performance of BCJ under cyclic loading with the formation of hinges in columns [29,30]. Roy and Laskar [31] experimentally investigated the behavior of GFRP-strengthened exterior BCJ with an introduction of construction joint in the lower column. The GFRP sheets were applied in an L-shaped configuration on the interior face and straight on the exterior face of the column covering the construction joint. The authors concluded that the GFRP application remarkably improved the stiffness, ductility and energy dissipation capacity as well as changing failure mode by hinge formation

in the beam rather in the column. Yu et al. [32] repaired ten damaged interior BCJ with viscous epoxy and, subsequently, strengthened it through FRP composites applied in an L-shaped pattern. The experimental data revealed that the strength and deformability of all the strengthened BCJ were regained and improved. Furthermore, a numerical formula was suggested for the accurate prediction of the efficiency of the BCJ strengthened with the L-shaped FRP sheets. The effect of bonding FRP composites in two different schemes (joint, beam and portion of column versus joint region only) was investigated for the interior RC BCJ [33], exterior RC BCJ [34], and corner RC BCJ [35]. In these studies, applications of the CFRP sheets in a specified layout and mechanical anchorage effect on the debonding were evaluated. The results indicated that the strengthening of joints along with adjacent connected RC members was highly effective in improving the strength parameters of BCJ which lacked transverse reinforcement. Furthermore, the importance of mechanical anchorage for mitigating debonding was highlighted. Mahini and Ronagh [36,37] conducted experiments on the web-bonded FRP configuration used for retrofitting the poorly detailed BCJ tested with a monotonic and cyclic loading protocol. The test results showed that the web-bonded FRP composites were a successful solution for repositioning the hinge away from the column to the beam. Also, the web-bonded FRP composites increased the initial stiffness of the retrofitted BCJ; however, no noticeable improvement was observed in strength. On the other hand, bonding of the FRP composites to the flange substantially improved the performance of seismically deficient BCJ [38–40].

FRP composites are widely used for strengthening RC members or structures due to its numerous favorable characteristics [41,42]; however, the predominant failure mode of the FRP composites, i.e., debonding of the FRP sheets/strips from the concrete substrate, is a prime concern related to its application. The debonding phenomena impair the performance of the FRP composites by detaching from the concrete substrate well before reaching their ultimate capacity. To avoid debonding and achieve maximum utilization of the FRP composites' tensile capacity, various anchorage techniques have been proposed [21,26,33,34,41,43,44]. However, in most of the techniques, a combination of external anchorage devices or steel assemblies was proposed, requiring an artful intervention in the existing RC members and also disturbing the intended serviceability of structures. Another practically applicable approach for the elimination of the debonding and improving anchorage is the concrete surface preparation and use of FRP anchors. In this regard, Gergely et al. [45] studied different surface preparation methods to improve the bond between concrete and FRP composites. It was concluded that the high-pressure water jet, in combination with the high-strength adhesive, achieved better bonding of the FRP composites. Likewise, Mostofinejad and Akhlaghi [46] investigated the performance of the externally bonded reinforcement on grooves (EBROG) technique along with the FRP anchors in the shear deficient BCJ. In this technique, grooves of the specified dimensions were made on the concrete surface to achieve a higher bond area between the concrete and the FRP composites. The FRP anchors were adopted to prevent the concrete cover from splitting. The test concluded that the EBROG technique combined with the FRP anchors has successfully eradicated the debonding failure of the FRP composites and enhanced the seismic capacity of the BCJ. A similar study was conducted by Ilia et al. [47] using the EBROG technique in combination with FRP anchors in the X-shaped layout to strengthen the deficient BCJ. It was concluded that the EBROG technique along with other combinations successfully eliminated the debonding of the FRP composites and improved the strength characteristics of the weak column-strong beam joints. Furthermore, the importance of strengthening beams connected to the joint was highlighted for shifting the hinges formation away from the column and joint.

A thorough review of the literature reveals that FRP composites are most widely used for the rehabilitation of deficient BCJ in RC buildings [5]. Although the FRP composites can enhance the seismic performance of the BCJ, debonding from the concrete surface impedes their capability to improve the strength characteristics. Moreover, most of the proposed anchorage techniques for the FRP composites are limited to the two-dimensional (2D) BCJ,

involving an artful intervention, and requiring a prolonged application time. Therefore, the main focus of this study is to investigate an effective, easy, and practically applicable method for installing FRP composites to eliminate debonding and improve the strength characteristics of the deficient BCJ. For this purpose, a practical anchorage methodology was adopted to avoid debonding of the L-shaped CFRP sheets (LCS) in the deficient BCJ. The LCS were anchored at the beam-column interface and at the far ends in the beam and column. For the experiment, two 1/3rd scaled, two-story RC frame structures were built to represent a three-dimensional (3D) RC structure with seismically deficient BCJ. One of the RC frame structures was tested as a control test frame, whereas the second one was strengthened with the FRP composites applied in the L-shaped layout in the BCJ. Both frames were loaded laterally using a cyclic reversed loading. The response of the FRP composites, failure pattern, lateral load-displacement behavior, and other relevant characteristics are presented and analyzed.

2. Experimental Program

2.1. RC Frame Description

In this study, a two-story RC moment frame building, usually practiced for low-rise public buildings, was considered for testing. The frame consists of two stories, a single bay in one direction and two bays in the other direction, with a spacing of almost 5.5 m and a floor height of 3.6 m, as shown in Figure 1. This study focused on the assessment of the central frame within this building.

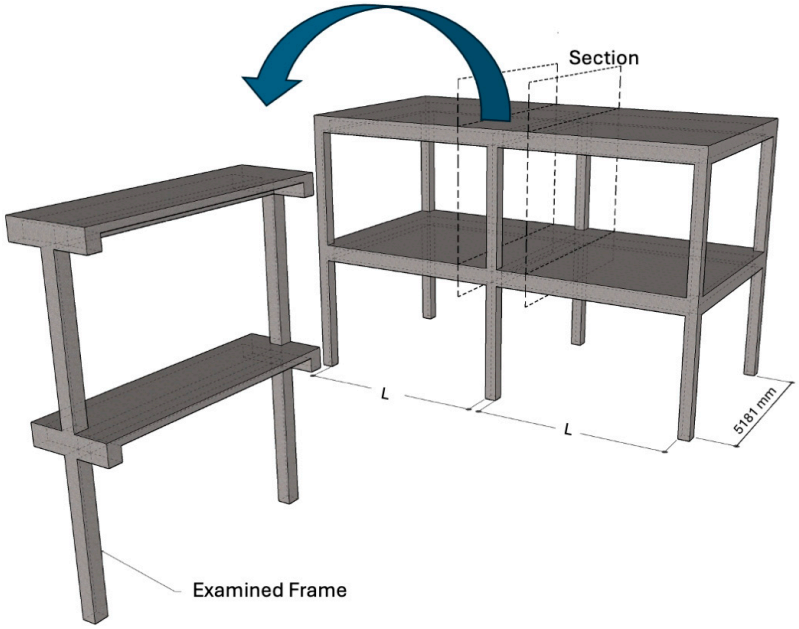

Figure 1. Plan view of the prototype building.

The RC members of the test frame were detailed to represent typical deficient members observed in buildings built before the development of seismic codes. However, for the scope of this study, only shear deficient BCJ and weak column-strong beam conditions were analyzed. To guarantee a shear-deficient behavior of beam–column joints (BCJ), transverse reinforcement was intentionally omitted in the joints of the frame. Conversely, to meet the strong beam–weak columns condition, the reinforcement in columns was specifically designed to ensure a lower flexural capacity than that of the beams. Therefore, a 305 mm × 457 mm (12 in × 18 in) beams (longitudinal + transverse) reinforced with 6Ø19 (#6) longitudinal rebars (bottom + top layers) and confined by Ø10 mm (#3) rebars provided at a spacing of 152.4 mm (6 in) center to center. Columns 305 mm × 305 mm (12 in × 12 in) reinforced with 8 Ø19 mm (#6) longitudinal rebars and Ø10 mm (#3) rebars as shear reinforcement at a spacing of 152.4 mm (6 in) center to center were provided. The

slab had a thickness of 152.4 mm (6 in), reinforced with Ø12 mm (1/2 in) deformed bars in two layers, in both directions, at a spacing of 152.4 mm (6 in) center to center. The concrete cover in beams and columns was 37.5 mm (1.5 in), whereas, for slab, the cover was 32 mm (1 and ¼ in) to allow concrete under reinforcement in the reduced scaled test frame. The reinforcement details of the prototype building are shown in Figure 2.

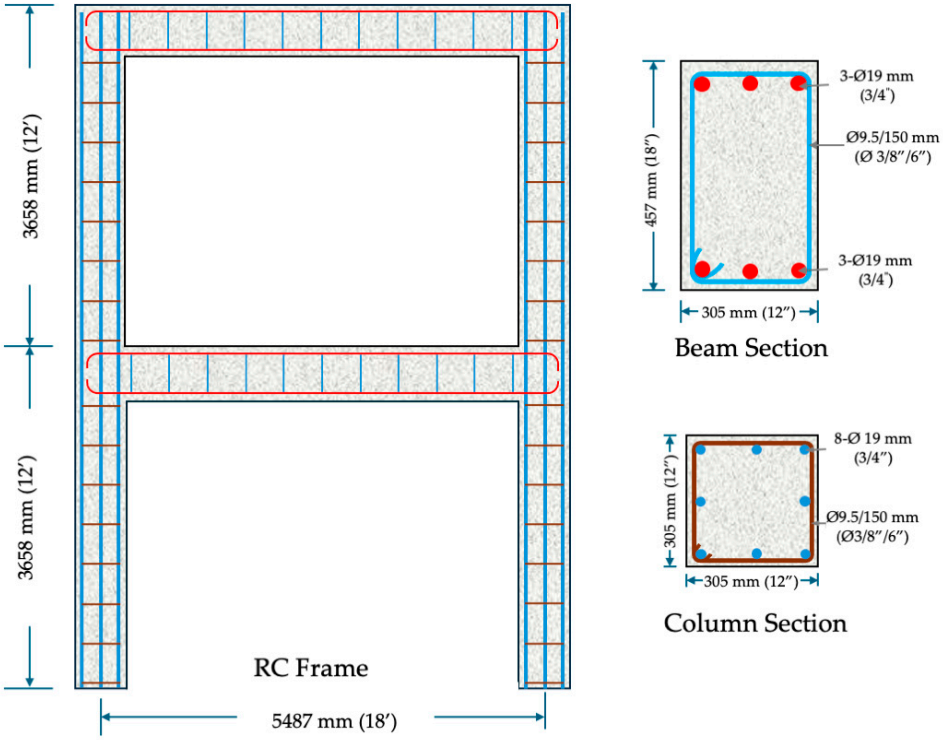

Figure 2. Reinforcement details of the prototype frame.

The flexural strength ratios for columns and beams adjacent to the ground-story joint were calculated in accordance with Section 18.7.3.2 of ACI-318-14 [48]:

$$\frac{\Sigma M_{nc}}{\Sigma M_{nb}} \geq 1.2 \quad (1)$$

where ΣM_{nc} and ΣM_{nb} are the sums of the flexural strength of the columns and the beams connected to a particular joint, respectively. The flexural strength calculated for the columns and the beams with given reinforcement resulted a value of 0.72, which is lower than the 1.2 mentioned in (1). Thus, a weak column–strong beam condition was ensured.

A one-bay frame in the critical direction representing the actual 3D structure was selected as an experimental frame. The test frame was reduced by 1/3rd scale and identical to Frame 4 used in the previous study [49]; however, to study the effect of the proposed layout of FRP composites and anchorage, an important modification was made in lower story column sizes. The rationale for the modification lies in the fact that, under lateral loading, the base of ground-story columns experiences a higher bending moment. This, in turn, causes concrete cracking and the formation of flexure hinges well in advance of hinge development elsewhere in the frame. Consequently, it leads to a complete loss of capacity [49]. The flexure-hinge formation will result in a free rotation of the structure without resisting any lateral load, although the ground story joints' strength didn't substantially deteriorate. As the objective of this paper is to assess the performance of L-shaped FRP configuration and anchorage in ground story joints, the ground story columns in the test frame were enhanced from 203 mm × 203 mm (8″ × 8″) to the height of 609.6 mm (24 in) from the base as shown in Figure 2. This modification would ensure that the bending moment caused by the lateral load at the interface of ground floor columns is lower than

that at the first-floor column base. The thickened column was reinforced with 8 Ø10 mm (#3) longitudinal rebars, and one Ø3 mm (#1) rebar as a transverse reinforcement was provided at a spacing of 50.8 mm (2″) all over the column. The size of the members of the prototype and test frame are presented in Table 1. The RC frame used in the study is shown in Figure 3.

Table 1. Dimensions of prototype and test frame.

Geometric Dimensions		
	Prototype	**Test Frame (1:3 Scale)**
Beam Dimensions	305 mm × 457 mm (12 in × 18 in)	102 mm × 152.4 mm (4 in × 6 in)
Column Dimensions	305 mm × 305 mm (12 in × 12 in)	102 mm × 102 mm (4 in × 4 in)
Slab Dimensions	152.4 mm (6 in)	50.8 mm (2 in)

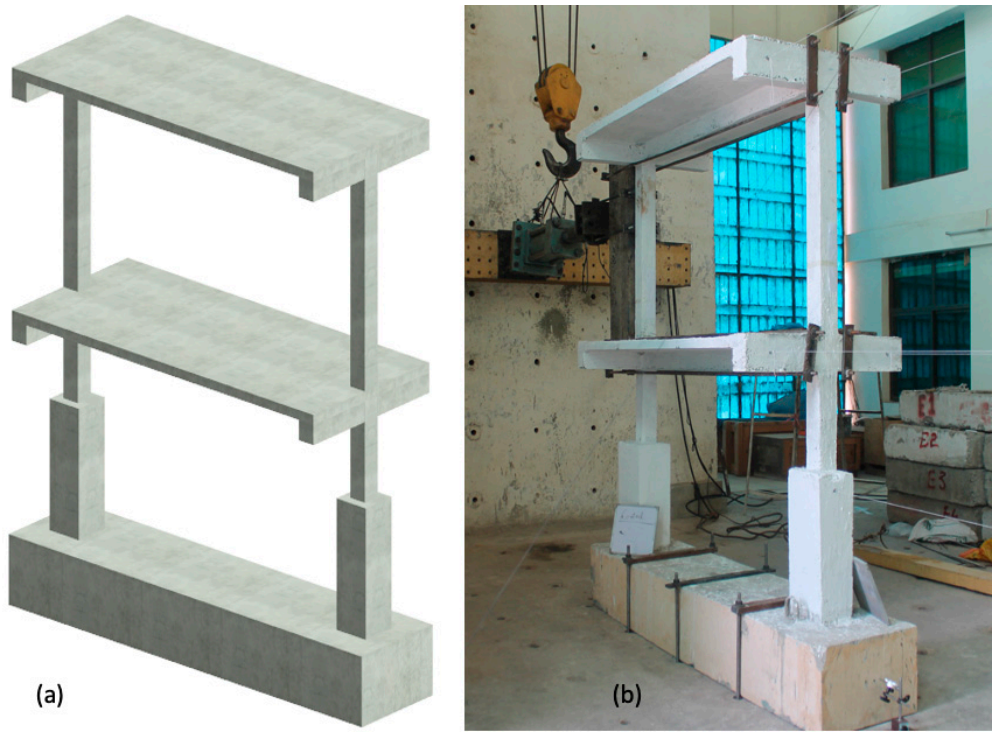

Figure 3. Test frame; (**a**) perspective view, and (**b**) control frame.

2.2. Material Properties

The normal-weight concrete with 28 days cylinder compressive strength of 13.8 MPa (2000 psi) was used in the test frame. The ACI mix design procedure was adopted to find proportions for concrete [50]. The maximum dimension of coarse aggregate was limited to 8 mm, keeping in view the least dimension of the slab in the test frame. The cylindrical concrete specimens 150 mm × 300 mm (6 by 12 in) were cast during the construction of the test frame and tested at the time of cyclic testing. Similarly, the 3 mm and 6 mm rebars resulted in yield strengths of 456 MPa and 445 MPa, respectively. The mechanical properties of the steel reinforcement are presented in Table 2.

Table 2. Properties of the reinforcement used in the test frame.

Rebar Diameter (mm)	Yield Strength (MPa)	Ultimate Strength (MPa)	Yield Strain (%)	Ultimate Strain (%)	Elastic Modulus (GPa)
3	456	592	1.67	17.36	218
6	445	569	1.82	20.80	207

Unidirectional carbon fiber fabric, Sika Wrap-230 C, was used in the LCS and wrapping. The pultruded carbon fiber plates (laminate), Sika Carbodur-S-812, were used as a CFRP laminate on the outer face of columns. Two types of adhesives were employed in this study. The Sikadur-330 is essentially a two-part impregnation primer resin used for bonding CFRP sheets to concrete surfaces, whereas the Sikadur-30 LP was used for bonding the CFRP laminates. The mechanical properties of fibers and resin are reported in Table 3.

Table 3. Properties of the FRP composites and resins.

Material	Tensile Modulus (GPa)	Tensile Strength (MPa)	Ultimate Tensile Strain (%)	Thickness (mm)
CFRP Sheet (SikaWrap-230 C)	230	4000	1.70	0.129
CFRP Laminate (Sika CarboDur S-812)	165	3100	1.80	1.20
Primer Resin (Sikadur-330)	4.5	30	0.90	-
Adhesive (Sikadur-30 LP)	10	17	-	-

2.3. Preliminary Design of FRP Composite Retrofit Scheme

To assess the effectiveness of L-shaped CFRP sheets (LCS), only the BCJ of the ground floor slab was strengthened with LCS. To avoid debonding of the FRP composites, which is most likely to occur at the beam–column interface [24,47], a narrow opening in the slab adjacent to the beam along with complete wrapping around the L-shaped FRP sheets were proposed. The ACI 440.2R also suggests the superior performance of a complete wrapping around the perimeter of the strengthened section [51]. A narrow opening (300 mm long × 8 mm wide), in a ground floor slab adjacent to the beam-column interface and extending to the far end, where the L-shaped CFRP sheet terminates, was produced by a machine grinder with a steel disc, as shown in Figure 4. These slots were made flush to the beam on both sides.

Figure 4. Opening in slab for aiding complete wrapping, (**a**) above joint and (**b**) below joint.

One of the main objectives of this study is to investigate the performance of the L-shaped FRP configuration for enhancing the seismic capacity of deficient BCJ. To achieve this objective, two L-shaped unidirectional CFRP sheets (80 mm wide × 0.129 mm thick) were attached at the beam-column interface and extended to a length of 300 mm on the column and beam flanges above and below the joints, respectively, as shown in Figure 5. The extended bonded length (300 mm) of the LCS on the columns and beams was to ensure the development of the full strength of FRP, as recommended by Section 14.1.3 of ACI 440.2R-17 [51]. The wrapping around the L-shaped CFRP sheets was accomplished with a 50 mm (2″) wide CFRP sheet applied in a double layer adjacent to the beam-column interface. In contrast, a single layer was applied at the far ends of the beams and columns to resist peel-off, respectively. The external face of columns, including the ground floor joints, was strengthened by a single CFRP laminate (80 mm wide × 1.2 mm thick) possessing a higher axial rigidity (3 times) than the internal LCS combinedly. The authors believe that the true response of the LCS will be captured if a higher axial rigidity CFRP laminate is attached to the external face, which will ensure rupture failure of the CFRP sheets prior to the CFRP laminate. Furthermore, if the CFRP laminate fractures before the LCS, it is probable that the RC column will be compelled to bear larger bending moments, potentially resulting in the development of flexure hinges in the column. The flexure-hinge formation will significantly reduce the lateral-load capacity; therefore, the true performance of LCS configuration will not be assessed completely. Moreover, a single 50 mm CFRP sheet was wrapped in the column hinge regions to increase the ductility, as suggested by Section 13.3.2 of ACI 440.2R-17 [51]. This strategy was derived from the observed behavior of the control frame during testing, where flexure hinges were initiated in the column hinge region. To mitigate debonding, a wrapping layout, as discussed above, was employed. It must be noted that no strengthening was employed for the first story joints, other than a wrapping that was applied on the end of the CFRP laminate, as this study focused on assessing LCS performance. The proposed layout for installation of externally bonded FRPs is shown in Figure 5.

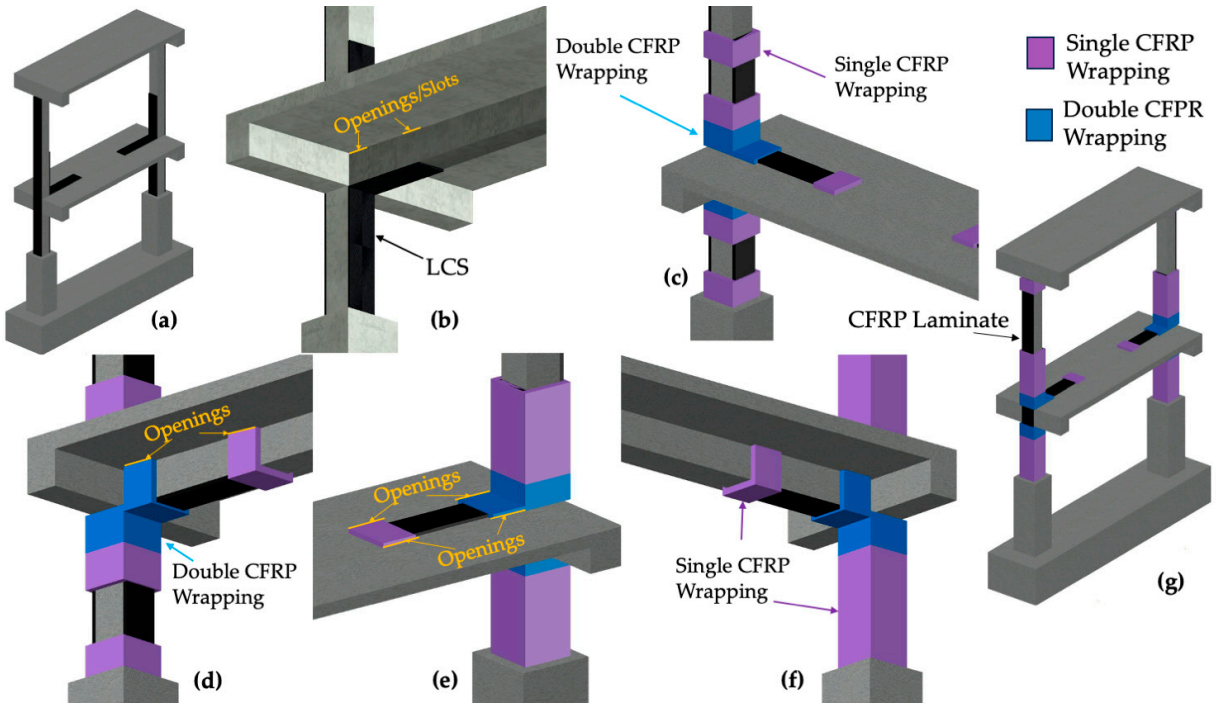

Figure 5. Proposed FRP layouts for strengthening (**a**) CFRP laminate on the outer face of the column, (**b**) LCS below joint, (**c**–**f**) wrapping of CFRP sheets, and (**g**) perspective view of the proposed FRP strengthening scheme.

2.4. Installation of FRP Sheets and Laminates

Once the proposed openings were incorporated, the concrete substrate (surface) was smoothed by a harsh sandpaper disc mounted on a grinder machine. Subsequently, all the sharp edges of beams and columns were rounded by a radius of 15 mm, as recommended, to elude stress concentration in wrapping sheets [51]. Afterwards, a Sikadur-30 LP adhesive was applied on the external face to bond the CFRP laminates, and Sikadur-330 primer resin was applied on the internal faces to bond the LCS to the concrete substrate. Upon applying the adhesives, the initial layer of the LCS was placed both above and below the joints. Subsequently, primer resin was applied to facilitate the curing process. Meanwhile, the CFRP laminates were bonded to the outer face of the columns. Afterwards, the second layer of the LCS was applied in the respective locations. Finally, for anchorage, the CFRP sheets (50 mm wide) were wrapped around the proposed locations. More specifically, the CFRP was initially cut to the required length (twice the perimeter plus the depth of the beam). The CFRP sheet was applied around the beam, through the openings starting from the lower corner of the beam's side and finishing at the top of the same side. In order to avoid premature failure of the FRP fabric at the concrete corners, the concrete surface of the beam at the slot was rounded using a grinder to a 15 mm radius. A detailed view of the systematic application of the proposed FRP scheme is shown in Figure 6.

Figure 6. FRP application procedure (**a**) smooth concrete surface, (**b**) adhesive applied on the surface, (**c**) LCS installed, (**d**) CFRP laminate on the outer face of the column, (**e**) complete wrapping below joint, (**f**) complete wrapping around column, (**g**) view of strengthened joint, and (**h**) complete FRP strengthening scheme.

2.5. Experimental Setup

The test frame was placed for in-plane loading and locked to the strong floor to prevent any movement of the pad. A hydraulic actuator was assembled to a vertical steel distribution beam that was anchored to both floors of the test frame through steel plates and anchors. A hydraulic actuator was attached in this position to transmit the applied lateral load in a proportion of 2/3rd to the second floor and 1/3rd to the first floor. This force distribution is consistent with the vertical distribution of base shear over the structure height for the fundamental mode [52].

To obtain the test data, various data sensors, including displacement transducers, strain gauges and one load sensor, were installed at different locations on the frame. A

total of six displacement transducers (DT) were installed to record the displacement data of the test frame in the loading direction. Out of six, two DTs were placed at the ends of transverse beams on each floor, and one was positioned at the interface of the ground-story columns. Similarly, one DT was attached to the base of the foundation pad to measure any possible sliding movement. One strain gauge was installed on the flexural reinforcement of the beam and one on the column; however, during construction they were disturbed and malfunctioned. Therefore, strain data for reinforcement were not captured. The test setup and location of the data sensors of the test frame are shown in Figure 7.

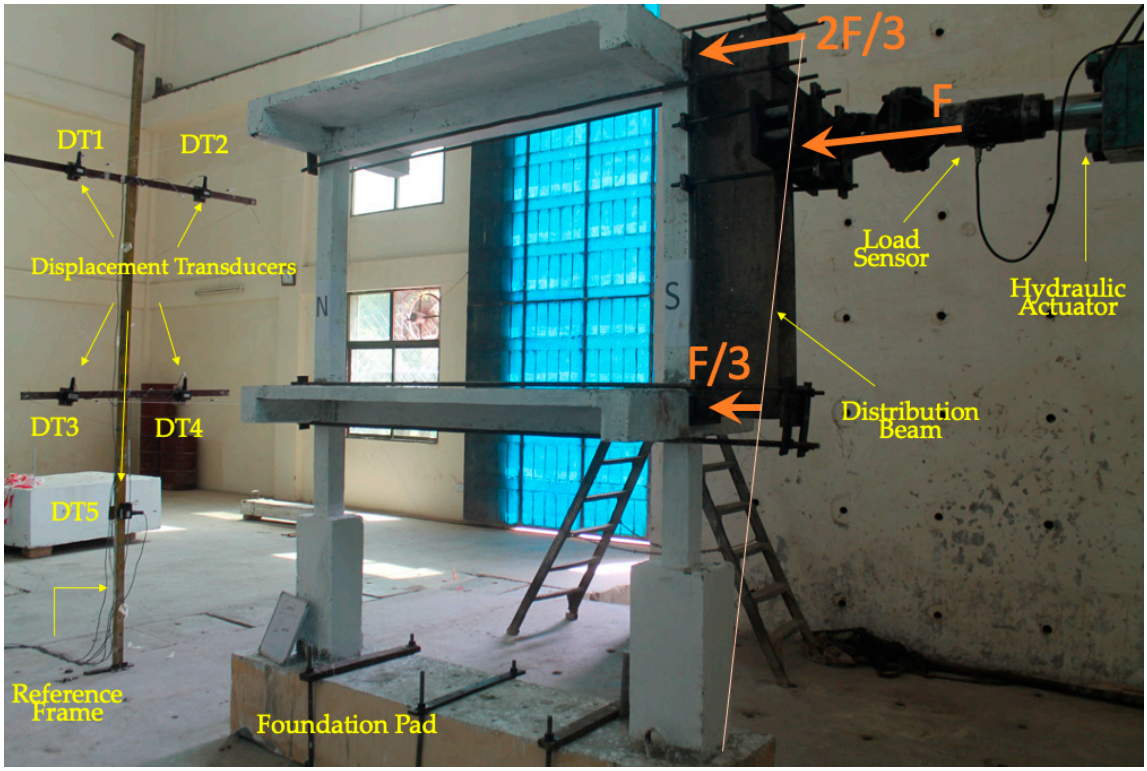

Figure 7. Test setup and instrumentation. Yellow color was used for description of experimental setup, while orange to indicate the applied loads. N and S are the names of the columns.

A lateral cyclic reversed loading with increasing amplitude was applied through a displacement-controlled actuator (200 kN). The loading history consists of a number of cycles of distinct displacement calculated from drift ratios based on recommendations of ACI Committee 374.1 [53]. At each displacement level, three complete reversible cycles were applied to the test frame. In the beginning, displacement corresponding to a drift ratio of 0.2% was adopted to check the linear elastic response of the test frame [46]. Afterwards, the amplitude of succeeding displacement levels was adjusted so that it was neither less than one and one-quarter times nor greater than one and one-half times the last displacement level [53]. At the end of three cycles, one corresponding to each displacement level, the test frame was examined for any damages that occurred. The applied lateral cyclic loading history is presented in Figure 8. It is worth mentioning that no additional axial load was applied on structure as it was not of much importance. For this study, the axial ratio was 0.012; however, the higher axial ratio would have favored the performance of FRP strengthened joints, as evident from a previous study [16].

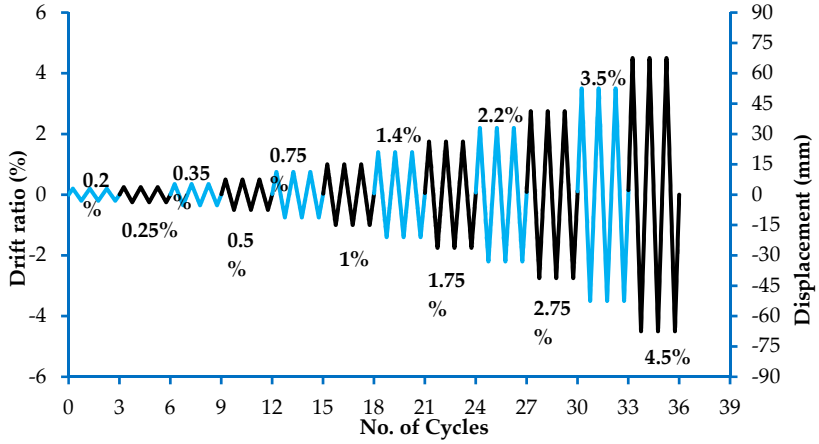

Figure 8. Reversed cyclic lateral loading program.

3. Results

3.1. Control Frame

In the very beginning, hair-line flexural cracks were observed in the base of the column at the first story when the lateral load corresponding to a drift ratio of 0.2% was applied. When the drift ratio reached 0.35%, a horizontal crack appeared at the construction joints of both columns at the first story. As the displacement level increased to a drift ratio of 0.75%, the flexural cracks in the columns widened, and the shear cracks generated in the transverse beams inclined to the axis of the beam. It was observed that, in 2D joints, X-shaped shear cracks usually appeared in joints [46], whereas in 3D joints, torsional shear cracks were induced in the transverse beams [54]. These existing cracks further propagated. A vertical crack appeared on both faces of columns along the loading direction, while at the ground-story column interfaces, flexural cracks developed when a drift ratio of 1.2% was applied. Further increasing the drift ratio to 1.75%, the joints in the first story substantially deteriorated, with a portion of concrete spalling; the concrete cover cracked in the first story column bottom, and the transverse beams significantly cracked. Finally, at the drift ratio of 2.2%, the concrete wedge separated from the ground-story joints, and concrete crushing was observed in first-story columns. At this stage, a sudden drop was observed in lateral load, and the test was stopped. The final damaged pattern observed in the control frame is shown in Figure 9.

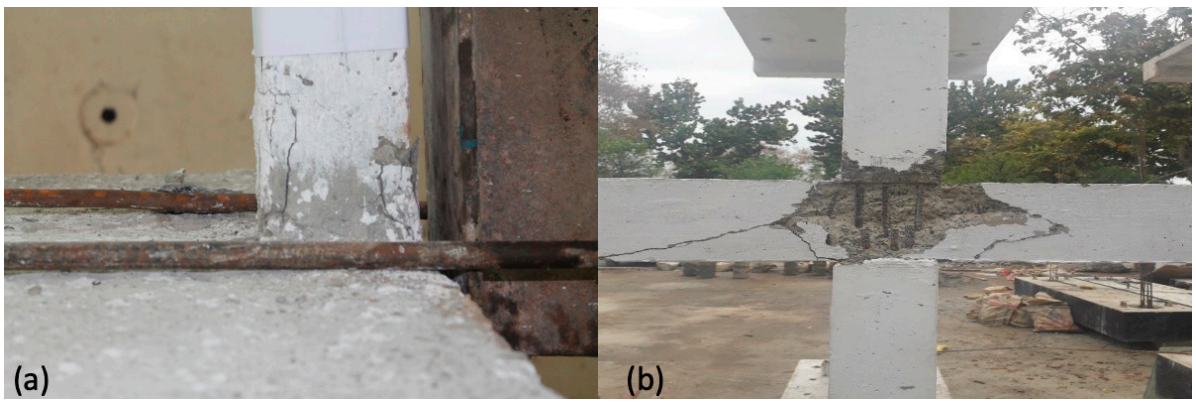

Figure 9. Failure pattern in the control frame, (**a**) flexural hinges in columns, and (**b**) shear failure of joint.

3.2. Strengthened Frame

The strengthened test frame shows a better response in the initial loadings up to a drift level of 0.5%, as no cracks were observed in the base of first-story columns. At the drift ratio of 0.5%, horizontal cracks were observed at the top construction joints of

first story columns and hair-line torsional shear cracks in transverse beams. It should be pointed out that transverse beams were not strengthened in this study. When the drift reached 1%, the cracks in transverse beams at both floors widened, and hair-line flexural cracks were observed at the interface of the columns in the ground story. At a drift of 1.75%, the joints on the 2nd floor experienced significant damage, with concrete spalling off. Additionally, a few fibers of LCS ruptured at one corner close to the beam-column interface. Moreover, flexural cracks at the interface of the columns in the ground story widened considerably, resulting in a noticeable detachment of a portion of the transverse beam. At a 2.2% drift ratio, the concrete completely spalled off from joints of the 2nd floor, a few hair-line cracks were observed in the ground floor beam, and the LCS further ruptured. When the lateral displacement level reached a drift of 3.0%, the LCS completely ruptured at the beam-column interface, and a few visible cracks were produced in the beams. Beyond the 3.0% drift ratio, the lateral load kept increasing due to the presence of CFRP laminates on the back side of the columns. Once the existing cracks at the interface of the column in the ground story closed, the CFRP laminates became active in resisting the lateral load. It should be noted that the rupture of LCS indicates that the proposed anchorage was successful in preventing debonding. Furthermore, the LCS relocated the flexural cracks into the beam. Finally, the test was stopped at a drift ratio of 3.5% due to the limitation of hydraulic actuator displacement capacity. The final damage pattern of the strengthened test frame is shown in Figure 10.

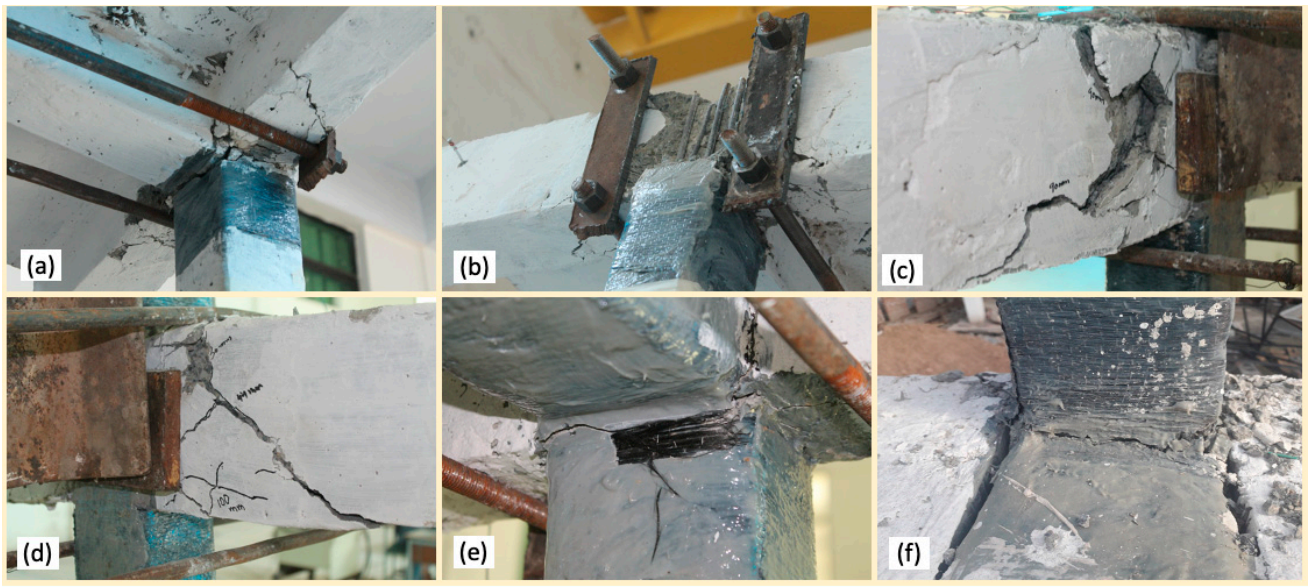

Figure 10. Failure pattern of the strengthened test frame, (**a**,**b**) second floor joint, (**c**,**d**) shear failure of the transverse beam, and (**e**) rupture of the LCS below the joint and (**f**) rupture of the LCS above the joint.

After the test, the LCS and laminates were removed to inspect damages in the concrete at joints, columns, and beams. No damage appeared in the concrete core of the joint, as seen in Figure 11a. However, a crack was observed at the top interface of beam–column joints, as seen in Figure 11b. Moreover, the column's flexural cracking was eliminated in the strengthened frame. This further justified the superior performance of the L-shaped CFRP configuration.

(**a**) (**b**)

Figure 11. Undamaged concrete, (**a**) in joint covered by CFRP laminate, and (**b**) above joint covered by L-shaped CFRP sheets.

3.3. Force Displacement Hysteretic Response

The force-displacement hysteresis curves play a crucial role in evaluating various aspects of RC members, including strength characteristics, ductility, energy dissipation capability, and the pinching behavior under lateral reversal loads. The force-displacement hysteresis curves for the control and strengthened frame are shown in Figure 12. For the control frame, the peak lateral load of 27.44 kN was recorded, corresponding to a drift ratio of 1.75%. A drop in lateral load was observed at the maximum drift ratio of 2.2%. The brittle failure of the control frame can be observed in the hysteresis curve, where a severe pinching phenomenon occurred [46]. It is obvious that the column flexural hinging and brittle shear failure of joints led to a non-ductile failure mode in the control frame.

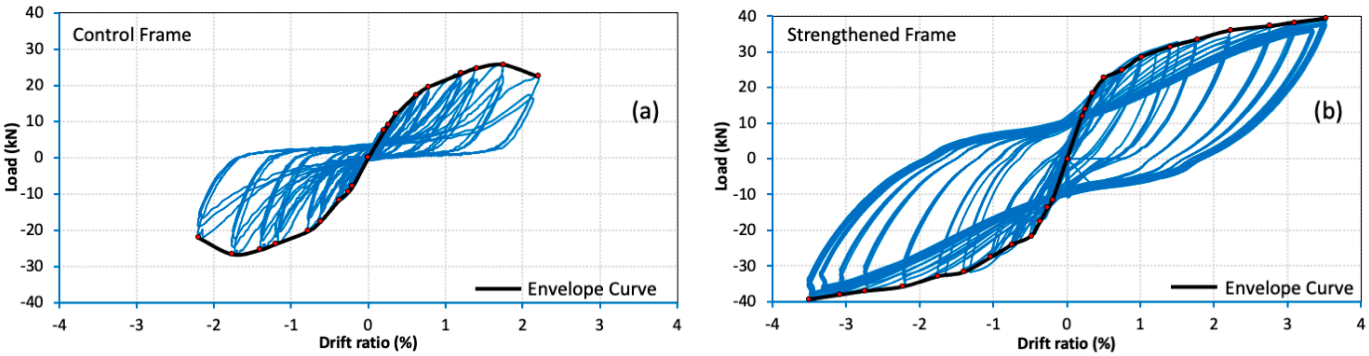

Figure 12. Force displacement hysteresis curves, (**a**) control test frame, and (**b**) strengthened test frame.

On the other hand, the strengthened frame accomplished a much better performance than the control frame in terms of lateral load capacity and failure mechanism. The presence of large hysteresis loops without a pinching effect confirms the ductile behavior of the strengthened frame [12,55]. The peak load in the strengthened frame reached 39.51 kN, corresponding to a drift ratio of 3.5%. The CFRP strengthening scheme increased the lateral load capacity by 45.9% and the drift by 43.1% as compared to the control frame. This shows that the L-shaped configuration of CFRP can successfully improve the strength and ductility characteristics.

3.4. Comparison of Force vs. Displacement Capacity Curves

The force-displacement envelope curves of the control and strengthened test frames are shown in Figure 13. It can be inferred that the LCS successfully enhanced the lateral

load-carrying capacity of the strengthened test frame by 45% compared to the control test frame. Moreover, the application of the LCS significantly increased the initial stiffness of the strengthened test frame. Moreover, the peak loads, ultimate loads, and the corresponding drift ratio of the test frames are summarized in Table 4.

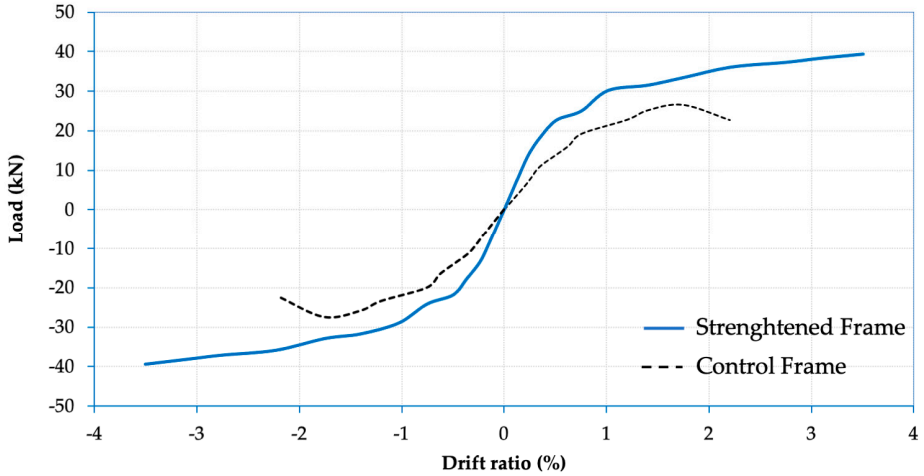

Figure 13. Comparison of force vs. displacement envelope curves.

Table 4. Summary of the results of tested frames.

Test Frame	Peak Load (kN)		Average (kN)	Peak Load Increase (%)	Drift at Peak Load (%)		Ultimate Load (kN)		Failure Mode
	(+)	(-)			(+)	(-)	(+)	(-)	
Control	26.49	27.44	26.97	-	1.74	1.76	22.68	22.28	-Flexure hinging in columns -Shear failure of joint. (see Figure 9)
Strengthened	39.32	39.38	39.35	45.9	3.50	3.50	39.32	39.38	-Second floor joints cracking -Shear cracking in the transverse beams, -Rupture of the L-shaped CFRP sheets (see Figure 10)

4. Discussion

4.1. Ductility

Ductility is the ability of the structural components to undergo a substantial deformation in the inelastic region without significantly losing strength capacity. It allows the structure to dissipate significant amounts of energy during lateral cyclic loading [56]. The displacement ductility of a test frame can be computed as the ratio of ultimate displacement to the yield displacement, as mentioned in Equation (2):

$$\mu = \frac{\Delta_u}{\Delta_y} \quad (2)$$

where Δ_u and Δ_y represent the ultimate and yield displacements, respectively.

In this study, the authors estimated the yield displacement by adopting the equivalent energy method [57]. The ultimate displacement was taken corresponding to a point when the lateral load dropped to 85% of the peak load [58].

As indicated in Table 5, the L-shaped CFRP strengthening successfully improved the ductility of the test frame. The ductility of the strengthened frame was improved by 43% compared to the control test frame. Furthermore, the wrapping of CFRP sheets for improving anchorage serves a dual purpose, as the wrapping of the columns in the plastic

hinge region proves to be more effective in improving the inelastic deformation capacity of the RC frame [51,58].

Table 5. Ductility factors of the tested frames.

Test Frame	Δ_y (mm)	Drift at Δ_y (%)	Δ_u (mm)	Drift at Δ_u (%)	μ	Increment (%)
Control	11.24	0.73	33.48	2.16	2.97	-
Strengthened	12.40	0.80	52.70	3.40	4.25	43.10

4.2. Stiffness Degradation

The stiffness degradation curve of the tested frames, as shown in Figure 14, is drawn by connecting the maximum values in each lateral cyclic loading and is calculated as follows [46,59]:

$$K_i = \frac{P_i^+ - P_i^-}{D_i^+ - D_i^-} \quad (3)$$

where P_i^+ and P_i^- represent peak load in positive and negative cyclic loading directions, respectively, and D_i^+ and D_i^- are corresponding displacements in ith cycle.

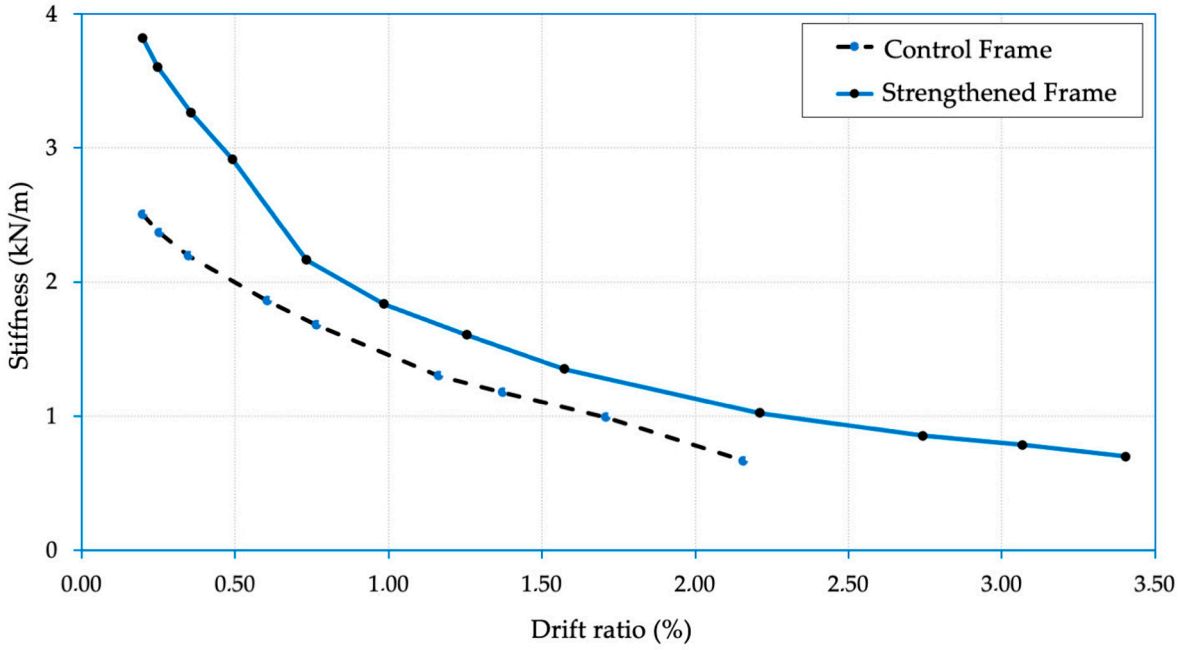

Figure 14. Stiffness degradation curves of the test frames.

Obviously, FRP strengthening enhanced the initial stiffness values of the RC frame compared to the control test frame. When the drift level increased, the stiffness decreased abruptly in the control test frame, whereas the stiffness of FRP-strengthened frame declined in a much more gradual manner. The gradual stiffness degradation is desirable in seismic events, as abrupt degradation often results in the collapse of RC structures [60].

4.3. Energy Dissipation

Energy dissipation capacity is essentially the ability of the structure to release the energy imparted during lateral loading [29]. In RC frame structure, the energy is dissipated by the formation of new cracks, friction between surfaces of existing cracks, and yielding of the steel reinforcement [55,60,61]. Debonding and rupture of CFRP sheets/strips in the strengthened RC structure can also lead to energy dissipation [61].

The cumulative dissipated energy refers to the total sum of energies dissipated during successive lateral loading cycles [29,55,62,63]. The cumulative dissipated energy versus

the drift ratio for the tested frames are shown in Figure 15. It is evident that the FRP-strengthened test frame demonstrated a higher cumulative energy dissipation capacity compared to the control test frame. This can be attributed to the larger areas enclosed by the large hysteresis loops in the CFRP-strengthened test frame.

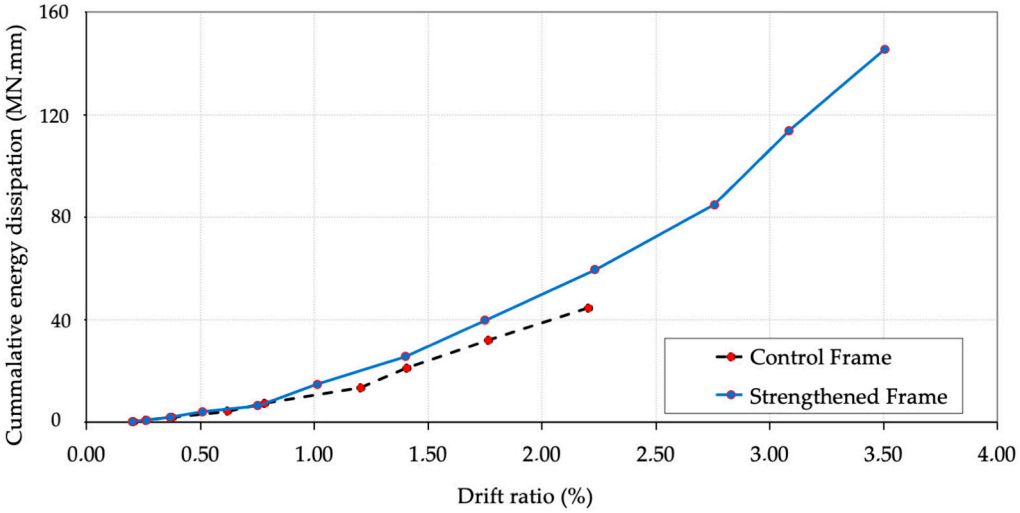

Figure 15. Energy dissipation capacities of the test frames.

4.4. Performance Levels

The performance levels developed for the tested RC frames according to the guidelines of FEMA-356 [64] are presented in Figure 16. Three performance levels, i.e., Immediate Occupancy (IO), Life Safety (LS), and Collapse Prevention (CP) limit state, were defined for the tested RC frames. Although the FRP-strengthened RC frame was able to undergo a second floor displacement corresponding to a drift ratio of 3.50%, the second floor joints were substantially damaged at a drift ratio of 2.20%. Thus, the latter was taken as the drift capacity corresponding to the CP limit state. The drift capacity corresponding to the LS limit state was equivalent to 75% of the drift capacity corresponding to the CP limit state. In contrast, for the IO limit state, it was estimated to be approximately 70% of the drift capacity corresponding to the LS limit state.

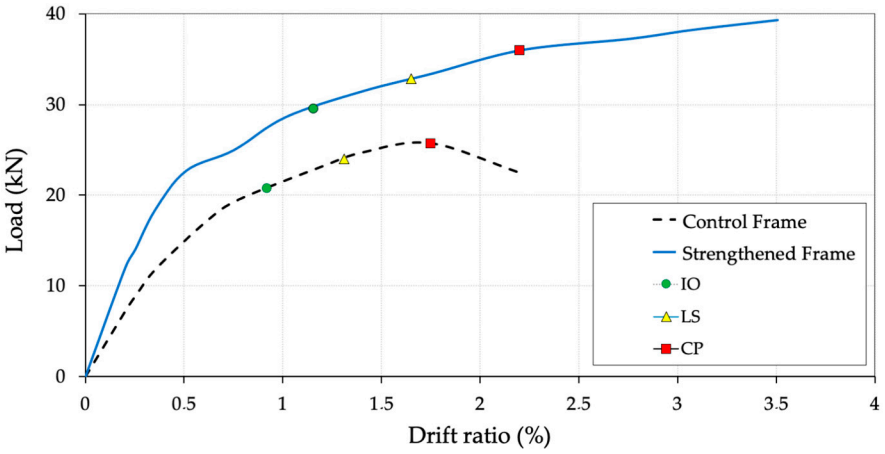

Figure 16. Performance limit states of the test frames.

From Figure 16, it can be observed that the CFRP strengthening successfully improved the CP limit state of the strengthened RC frame compared to the control test frame. The control test frame exhibited notable damage in the second floor joints, followed by deterioration in the ground story joints, resulting in a CP limit state at the maximum drift ratio of 1.75%. Conversely, in the strengthened test frame, the application of CFRP sheets improved

the strength of the ground-story joints and ductility. As a result, the CP limit state shifted to a higher drift ratio of 2.20%. This indicates that the CFRP-strengthened test frame could withstand a greater displacement level at the second floor before collapsing. Since the second floor joints in the CFRP strengthened test frame were significantly damaged as no strengthening scheme was applied, the authors posit that strengthening these joints could have substantially increased the drift capacity across different limit states.

5. Conclusions

This study presents the outcomes of an experimental study of a seismically deficient low-strength RC frame. The strengthening strategy employed L-shaped CFRP sheets in the ground-story BCJ, featuring improved anchorage to address debonding issues. For this purpose, two scaled RC test frames were detailed to represent the various seismic deficiencies, including strong beam–weak column and absence of the transverse reinforcement in the joints, were tested with lateral cyclic loading. The important findings from this experimental investigation can be summarized as follows:

- The suggested anchorage method, involving the creation of openings coupled with comprehensive wrapping, has eliminated debonding issues of the FRP composites. This has resulted in the rupture of the L-shaped CFRP sheets at the beam–column interface. Furthermore, the wrapping at the far end has averted the peel-off of the L-shaped CFRP sheets.
- The L-shaped CFRP sheets effectively improved the performance of the seismically deficient RC frame in terms of lateral load capacity, ductility, and energy dissipation capacity. The L-shaped CFRP sheets enhanced the lateral load capacity and ductility of the strengthened test frame by 45% and 43%, respectively. The higher energy dissipation capacity of the strengthened test frame could be attributed to higher ductility, imparted by the confining effect of CFRP wrapping in the hinge region of the columns.
- The L-shaped CFRP sheets successfully transformed the failure mechanism of the strengthened test frame from the brittle-shear failure of the joints, and the flexure hinging of columns into a significantly more ductile one, by relocating the formation of the hinges in the beams.

The authors suggest exploring the performance of alternative FRP configurations using similar frames. A parametric study involving different materials could prove to be highly beneficial as well.

Author Contributions: Conceptualization, W.A. and Q.A.; Methodology, W.A., F.U.R. and Q.A.; Validation, W.A., F.U.R., Q.A. and C.G.P.; Formal analysis, W.A., F.U.R., Q.A. and C.G.P.; Investigation, W.A., F.U.R. and Q.A.; Data curation, W.A., F.U.R., Q.A. and C.G.P.; Writing—original draft preparation, W.A.; Writing—review and editing, W.A., F.U.R., Q.A. and C.G.P.; Visualization, W.A., F.U.R., Q.A. and C.G.P.; Supervision, Q.A.; Project administration, W.A. All authors have read and agreed to the published version of the manuscript.

Funding: This research received no external funding.

Data Availability Statement: The original contributions presented in the study are included in the article, further inquiries can be directed to the corresponding author.

Conflicts of Interest: The authors declare no conflicts of interest.

References

1. Zhao, B.; Taucer, F.; Rossetto, T. Field Investigation on the Performance of Building Structures during the 12 May 2008 Wenchuan Earthquake in China. *Eng. Struct.* **2009**, *31*, 1707–1723. [CrossRef]
2. Pakzad, A.; Khanmohammadi, M. Experimental Cyclic Behavior of Code-Conforming Exterior Wide Beam-Column Connections. *Eng. Struct.* **2020**, *214*, 110613. [CrossRef]
3. Duan, H.; Hueste, M.B.D. Seismic Performance of a Reinforced Concrete Frame Building in China. *Eng. Struct.* **2012**, *41*, 77–89. [CrossRef]

4. Chung, L.L.; Chen, Y.T.; Sun, C.H.; Lien, K.H.; Wu, L.Y. Applicability Investigation of Code-Defined Procedures on Seismic Performance Assessment of Typical School Buildings in Taiwan. *Eng. Struct.* **2012**, *36*, 147–159. [CrossRef]
5. Tsonos, A.G. Effectiveness of CFRP-Jackets and RC-Jackets in Post-Earthquake and Pre-Earthquake Retrofitting of Beam-Column Subassemblages. *Eng. Struct.* **2008**, *30*, 777–793. [CrossRef]
6. Tsonos, A.D.G. Performance Enhancement of R/C Building Columns and Beam-Column Joints through Shotcrete Jacketing. *Eng. Struct.* **2010**, *32*, 726–740. [CrossRef]
7. Torabi, A.; Maheri, M.R. Seismic Repair and Retrofit of RC Beam-Column Joints Using Stiffened Steel Plates. *Iran. J. Sci. Technol. Trans. Civ. Eng.* **2017**, *41*, 13–26. [CrossRef]
8. Ruiz-Pinilla, J.G.; Cladera, A.; Pallarés, F.J.; Calderón, P.A.; Adam, J.M. RC Columns Strengthened by Steel Caging: Cyclic Loading Tests on Beam-Column Joints with Non-Ductile Details. *Constr. Build. Mater.* **2021**, *301*, 124105. [CrossRef]
9. Esmaeeli, E.; Danesh, F.; Tee, K.F.; Eshghi, S. A Combination of GFRP Sheets and Steel Cage for Seismic Strengthening of Shear-Deficient Corner RC Beam-Column Joints. *Compos. Struct.* **2017**, *159*, 206–219. [CrossRef]
10. Campione, G.; Cavaleri, L.; Papia, M. Flexural Response of External R.C. Beam-Column Joints Externally Strengthened with Steel Cages. *Eng. Struct.* **2015**, *104*, 51–64. [CrossRef]
11. Khodaei, M.; Saghafi, M.H.; Golafshar, A. Seismic Retrofit of Exterior Beam-Column Joints Using Steel Angles Connected by PT Bars. *Eng. Struct.* **2021**, *236*, 112111. [CrossRef]
12. Maddah, A.; Golafshar, A.; Saghafi, M.H. 3D RC Beam–Column Joints Retrofitted by Joint Enlargement Using Steel Angles and Post-Tensioned Bolts. *Eng. Struct.* **2020**, *220*, 110975. [CrossRef]
13. Tavasoli, E.; Rezaifar, O.; Kheyroddin, A. Seismic Performance of RC Joints Retrofitted by External Diagonal Bolts. *J. Build. Eng.* **2022**, *46*, 103691. [CrossRef]
14. Karayannis, C.G.; Sirkelis, G.M. Strengthening and Rehabilitation of RC Beam–Column Joints Using Carbon-FRP Jacketing and Epoxy Resin Injection. *Earthq. Eng. Struct. Dyn.* **2008**, *37*, 769–790. [CrossRef]
15. Khan, M.I.; Al-Osta, M.A.; Ahmad, S.; Rahman, M.K. Seismic Behavior of Beam-Column Joints Strengthened with Ultra-High Performance Fiber Reinforced Concrete. *Compos. Struct.* **2018**, *200*, 103–119. [CrossRef]
16. Antonopoulos, C.P.; Triantafillou, T.C. Experimental Investigation of FRP-Strengthened RC Beam-Column Joints. *J. Compos. Constr.* **2003**, *7*, 39–50. [CrossRef]
17. Täljsten, B. Strengthening Concrete Beams for Shear with CFRP Sheets. *Constr. Build. Mater.* **2003**, *17*, 15–26. [CrossRef]
18. Del Vecchio, C.; Di Ludovico, M.; Prota, A.; Manfredi, G. Modelling Beam-Column Joints and FRP Strengthening in the Seismic Performance Assessment of RC Existing Frames. *Compos. Struct.* **2016**, *142*, 107–116. [CrossRef]
19. Papakonstantinou, C.G.; Balaguru, P.N.; Auyeung, Y. Influence of FRP Confinement on Bond Behavior of Corroded Steel Reinforcement. *Cem. Concr. Compos.* **2011**, *33*, 611–621. [CrossRef]
20. Papakonstantinou, C.G.; Petrou, M.F.; Harries, K.A. Fatigue Behavior of RC Beams Strengthened with GFRP Sheets. *J. Compos. Constr.* **2001**, *5*, 22178. [CrossRef]
21. Ghobarah, A.; El-Amoury, T. Seismic Rehabilitation of Deficient Exterior Concrete Frame Joints. *J. Compos. Constr.* **2005**, *9*, 408–416. [CrossRef]
22. Ilia, E.; Mostofinejad, D. Seismic Retrofit of Reinforced Concrete Strong Beam–Weak Column Joints Using EBROG Method Combined with CFRP Anchorage System. *Eng. Struct.* **2019**, *194*, 300–319. [CrossRef]
23. Attari, N.; Amziane, S.; Chemrouk, M. Efficiency of Beam-Column Joint Strengthened by FRP Laminates. *Adv. Compos. Mater.* **2010**, *19*, 171–183. [CrossRef]
24. Le-Trung, K.; Lee, K.; Lee, J.; Lee, D.H.; Woo, S. Experimental Study of RC Beam-Column Joints Strengthened Using CFRP Composites. *Compos. Part B Eng.* **2010**, *41*, 76–85. [CrossRef]
25. Sezen, H. Repair and Strengthening of Reinforced Concrete Beam-Column Joints with Fiber-Reinforced Polymer Composites. *J. Compos. Constr.* **2012**, *16*, 499–506. [CrossRef]
26. Ghobarah, A.; Said, A. Seismic Rehabilitation of Beam-Column Joints Using FRP Laminates. *J. Earthq. Eng.* **2001**, *5*, 113–129. [CrossRef]
27. Manos, G.C.; Katakalos, K.; Koidis, G.; Papakonstantinou, C.G. Shear Strengthening of R/C Beams with FRP Strips and Novel Anchoring. *J. Civ. Eng. Res.* **2012**, *2*, 73–83. [CrossRef]
28. Manos, G.C.; Katakalos, K.; Papakonstantinou, C.G. Shear Behavior of Rectangular Beams Strengthened with Either Carbon or Steel Fiber Reinforced Polymers. *Appl. Mech. Mater.* **2011**, *82*, 571–576. [CrossRef]
29. Roy, B.; Laskar, A.I. Cyclic Behavior of In-Situ Exterior Beam-Column Subassemblies with Cold Joint in Column. *Eng. Struct.* **2017**, *132*, 822–833. [CrossRef]
30. Roy, B.; Laskar, A.I. Beam–Column Subassemblies with Construction Joint in Columns above and below the Beam. *Mag. Concr. Res.* **2018**, *70*, 71–83. [CrossRef]
31. Roy, B.; Laskar, A.I. Cyclic Performance of Beam-Column Subassemblies with Construction Joint in Column Retrofitted with GFRP. *Structures* **2018**, *14*, 290–300. [CrossRef]
32. Yu, J.; Shang, X.; Lu, Z. Efficiency of Externally Bonded L-Shaped FRP Laminates in Strengthening Reinforced-Concrete Interior Beam-Column Joints. *J. Compos. Constr.* **2016**, *20*, 04015064. [CrossRef]
33. Almusallam, T.H.; Al-Salloum, Y.A. Seismic Response of Interior RC Beam-Column Joints Upgraded with FRP Sheets. II: Analysis and Parametric Study. *J. Compos. Constr.* **2007**, *11*, 590–600. [CrossRef]

34. Al-Salloum, Y.A.; Almusallam, T.H.; Alsayed, S.H.; Siddiqui, N.A. Seismic Behavior of As-Built, ACI-Complying, and CFRP-Repaired Exterior RC Beam-Column Joints. *J. Compos. Constr.* **2011**, *15*, 522–534. [CrossRef]
35. Alsayed, S.H.; Almusallam, T.H.; Al-Salloum, Y.A.; Siddiqui, N.A. Seismic Rehabilitation of Corner RC Beam-Column Joints Using CFRP Composites. *J. Compos. Constr.* **2010**, *14*, 681–692. [CrossRef]
36. Mahini, S.S.; Ronagh, H.R. Strength and Ductility of FRP Web-Bonded RC Beams for the Assessment of Retrofitted Beam-Column Joints. *Compos. Struct.* **2010**, *92*, 1325–1332. [CrossRef]
37. Mahini, S.S.; Ronagh, H.R. Web-Bonded Frps for Relocation of Plastic Hinges Away from the Column Face in Exterior RC Joints. *Compos. Struct.* **2011**, *93*, 2460–2472. [CrossRef]
38. Dalalbashi, A.; Eslami, A.; Ronagh, H.R. Numerical Investigation on the Hysteretic Behavior of RC Joints Retrofitted with Different CFRP Configurations. *J. Compos. Constr.* **2013**, *17*, 371–382. [CrossRef]
39. Eslami, A.; Ronagh, H.R. Experimental Investigation of an Appropriate Anchorage System for Flange-Bonded Carbon Fiber–Reinforced Polymers in Retrofitted RC Beam–Column Joints. *J. Compos. Constr.* **2014**, *18*, 04013056. [CrossRef]
40. Maheri, M.R.; Torabi, A. Retrofitting External RC Beam-Column Joints of an Ordinary MRF through Plastic Hinge Relocation Using FRP Laminates. *Structures* **2019**, *22*, 65–75. [CrossRef]
41. Lee, W.T.; Chiou, Y.J.; Shih, M.H. Reinforced Concrete Beam-Column Joint Strengthened with Carbon Fiber Reinforced Polymer. *Compos. Struct.* **2010**, *92*, 48–60. [CrossRef]
42. Davodikia, B.; Saghafi, M.H.; Golafshar, A. Experimental Investigation of Grooving Method in Seismic Retrofit of Beam-Column External Joints without Seismic Details Using CFRP Sheets. *Structures* **2021**, *34*, 4423–4434. [CrossRef]
43. Ceroni, F.; Pecce, M. Evaluation of Bond Strength in Concrete Elements Externally Reinforced with CFRP Sheets and Anchoring Devices. *J. Compos. Constr.* **2010**, *14*, 521–530. [CrossRef]
44. Ascione, L.; Berardi, V.P. Anchorage Device for FRP Laminates in the Strengthening of Concrete Structures Close to Beam-Column Joints. *Compos. Part B Eng.* **2011**, *42*, 1840–1850. [CrossRef]
45. Gergely, B.J.; Pantelides, C.P.; Reaveley, L.D. S Hear S Trengthening Rct-J Oints U Sing Cfrp C Omposites. *J. Compos. Constr.* **2000**, *4*, 56–64. [CrossRef]
46. Mostofinejad, D.; Akhlaghi, A. Experimental Investigation of the Efficacy of EBROG Method in Seismic Rehabilitation of Deficient Reinforced Concrete Beam-Column Joints Using CFRP Sheets. *J. Compos. Constr.* **2017**, *21*, 04016116. [CrossRef]
47. Ilia, E.; Mostofinejad, D.; Moghaddas, A. Cyclic Behavior of Strong Beam–Weak Column Joints Strengthened with Different Configurations of CFRP Sheets. *Arch. Civ. Mech. Eng.* **2020**, *20*, 31. [CrossRef]
48. *ACI 318-14*; Building Code Requirements for Structural Concrete. ACI: Farmington Hills, MI, USA, 2014; ISBN 9780870319303.
49. Rizwan, M. Performance—Based Seismic Assessment of RC SMRF Compliant & Noncompliant Structures. Ph.D. Thesis, University of Engineering & Technology, Peshawar, Pakistan, 2019.
50. *ACI PRC-211.1-91*; Standard Practice for Selecting Proportions for Normal, Heavyweight, and Mass Concrete. ACI: Farmington Hills, MI, USA, 1991; pp. 1–38.
51. *ACI 440.2R-17*; Guide for the Design and Construction of Externally Bonded FRP Systems for Strengthening Concrete Structures. ACI: Farmington Hills, MI, USA, 2017.
52. Ministry of Housing and Works; Government of Islamic Republic of Pakistan. *Building Code of Pakistan—Seismic Provisions*; Ministry of Housing and Works: Islamabad, Pakistan; Government of Islamic Republic of Pakistan: Islamabad, Pakistan, 2007.
53. *ACI 374.1-05*; Acceptance Criteria for Moment Frames Based on Structural Testing and Commentary. ACI: Farmington Hills, MI, USA, 2005.
54. Della Corte, G.; Barecchia, E.; Mazzolani, F.M. Seismic Upgrading of RC Buildings by FRP: Full-Scale Tests of a Real Structure. *J. Mater. Civ. Eng.* **2006**, *18*, 659–669. [CrossRef]
55. Akhlaghi, A.; Mostofinejad, D. Experimental and Analytical Assessment of Different Anchorage Systems Used for CFRP Flexurally Retrofitted Exterior RC Beam-Column Connections. *Structures* **2020**, *28*, 881–893. [CrossRef]
56. Priestley, P.; Paulay, T.; Priestley, M.J.N. *Seismic Design of Reinforced Concrete and Masonry Buildings*; Wiley: New York, NY, USA, 1992; pp. 12–13.
57. Hu, B.; Kundu, T. Seismic Performance of Interior and Exterior Beam–Column Joints in Recycled Aggregate Concrete Frames. *J. Struct. Eng.* **2019**, *145*, 04018262. [CrossRef]
58. Ma, C.; Wang, D.; Wang, Z. Seismic Retrofitting of Full-Scale RC Interior Beam-Column-Slab Subassemblies with CFRP Wraps. *Compos. Struct.* **2017**, *159*, 397–409. [CrossRef]
59. Mostofinejad, D.; Hajrasouliha, M. Shear Retrofitting of Corner 3D-Reinforced Concrete Beam-Column Joints Using Externally Bonded CFRP Reinforcement on Grooves. *J. Compos. Constr.* **2018**, *22*, 04018037. [CrossRef]
60. Al-Salloum, Y.A.; Siddiqui, N.A.; Elsanadedy, H.M.; Abadel, A.A.; Aqel, M.A. Textile-Reinforced Mortar versus FRP as Strengthening Material for Seismically Deficient RC Beam-Column Joints. *J. Compos. Constr.* **2011**, *15*, 920–933. [CrossRef]
61. Hashemi, S.M.; Tajmir Riahi, H. Seismic Performance of Reinforced Concrete Beam-Column Joints Strengthened with NSM Steel Bars and NSM CFRP Strips. *Structures* **2022**, *39*, 57–69. [CrossRef]
62. Alavi-Dehkordi, S.; Mostofinejad, D.; Alaee, P. Effects of High-Strength Reinforcing Bars and Concrete on Seismic Behavior of RC Beam-Column Joints. *Eng. Struct.* **2019**, *183*, 702–719. [CrossRef]

63. Mostofinejad, D.; Hajrasouliha, M. 3D Beam–Column Corner Joints Retrofitted with X-Shaped FRP Sheets Attached via the EBROG Technique. *Eng. Struct.* **2019**, *183*, 987–998. [CrossRef]
64. *FEMA-356*; Prestandard and Commentary for the Seismic Rehabilitation of Building. ASCE American Society of Civil Engineers: Washington, DC, USA, 2000.